Sensors and Actuators B 145 (2010) 174–180

Contents lists available at ScienceDirect

Sensors and Actuators B: Chemical

journal homepage: www.elsevier.com/locate/snb

Humidity sensing properties of ZnO nanoparticles synthesized by sol–gel process

A. Erol [a,*], S. Okur [b], B. Comba [a], Ö. Mermer [c], M.Ç. Arıkan [a]

[a] Istanbul University, Science Faculty, Physics Department, Vezneciler, 34134 Istanbul, Turkey
[b] Izmir Institute of Technology, Faculty of Science, Department of Physics Gülbahce Koyu Kampüsü, Urla, Izmir, 35430, Turkey
[c] Ege University, Electrical & Electronics Engineering Department, Bornova, 35100 Izmir, Turkey

ARTICLE INFO

Article history:
Received 16 July 2009
Received in revised form
22 November 2009
Accepted 23 November 2009
Available online 1 December 2009

Keywords:
ZnO
Sensor
Humidity sensor
Nanoparticle
Quartz crystal microbalance

ABSTRACT

ZnO nanoparticles have been synthesized by the sol–gel method with approximately 10 nm diameter and the humidity adsorption and desorption kinetics of ZnO nanoparticles were investigated by quartz crystal microbalance (QCM) technique. The morphology and crystal structure of the ZnO nanoparticles have been characterized by scanning electron microscopy (SEM) and X-ray diffraction (XRD), respectively. The roughness of the surface has been investigated using atomic force microscope (AFM). The dynamic Langmuir adsorption model was used to determine the kinetic parameters such as adsorption and desorption rates and Gibbs free energy under relative humidity between 45% and 88%. The relative sensitivity of the ZnO nanoparticles-based humidity sensor was determined by electrical resistance measurements. Our reproducible experimental results show that ZnO nanoparticles have a great potential for humidity sensing applications at room temperature operations.

1. Introduction

ZnO nanostructures are promising candidates for wide range of applications from optoelectronics to variety of sensors [1–3]. Sensors based on nanostructures exhibit better sensing properties than bulk or thin film counterparts due to their huge surface-to-volume ratio. The sensing properties of ZnO nanostructures are usually based on the highly active surface properties and the selective response to certain gases. Several studies have been carried out so far to monitor gas sensing properties of ZnO nanostructures with different morphologies showing that the ZnO nanostructures are very reactive for the gases such as CO [4], H_2 [5], CH_4 [6], benzene [7] and volatiles like ethanol and acetone [8]. Apart from gas and vapor sensing, humidity monitoring is also very important for human life, industries, and scientific applications. To date, there are only few investigations done concerning of humidity sensing properties of ZnO nanostructures with different morphologies such as nanorod [9], flower-like nanomaterials [10], tetrapods [11], nanosized clusters [12] and nanowires [13]. Zhang et al. investigated the humidity sensing properties of ZnO nanorods [9] and nanowires [13] and they showed that the resistances of ZnO nanowires and nanorod devices changed more than four times and two orders of magnitude, respectively, when exposed to moisture of 97% relative humidity. Zhou et al. [10] presented a wireless relative humidity sensor system prototype which based on quartz crystal microbalance (QCM) coated by flower-like ZnO nanostructures as sensing element and obtained a frequency shift about 900 Hz @ 80% relative humidity. Wang et al. [11] studied humidity sensing properties of Pd-doped ZnO nanotetrapods using QCM and found Pd doping could improve sensitivity and linearity of sensor and measured a frequency shift with around 5000 Hz @ 80% relative humidity. Yadav et al. [12] observed that the resistance of annealed ZnO nano-sized clusters at 550 °C changed about 25 times at 80% relative humidity.

It is well known that nanosized-based sensors provide larger response due to their high surface-to-volume ratio. Exposing surface area of the nanomaterials to target gas is very important factor affecting directly sensitivity of the sensor. Zero-dimensional (0D) nanostructures, that is nanodots, have larger active area comparing its 1D nanowire counterpart, therefore it is expected that sensor based on nanoparticles provides better sensitivity for gas sensing. Xu et al. [14] reported that the sensitivity of ZnO gas sensors increase with decreasing grain size.

In this work, we present characterization, humidity sensing properties, the theoretical analysis of adsorption–desorption kinetics of ZnO nanoparticles and response of ZnO nanoparticles-based humidity sensor. ZnO nanoparticles with a size about 10 nm were synthesized by sol–gel process. The morphology, surface roughness and crystal structure of ZnO nanostructures were analyzed by SEM, AFM and XRD, respectively. Humidity sensing capabilities of the ZnO nanoparticles were investigated by QCM technique with increasing relative humidity (RH) up to 90%. The adsorption and desorption kinetics of ZnO nanoparticles under varying humidity

* Corresponding author. Tel.: +90 212 455 57 00; fax: +90 212 455 57 00.
E-mail addresses: ayseerol@istanbul.edu.tr, ayseerol@gmail.com (A. Erol).

0925-4005/$ – see front matter © 2009 Elsevier B.V. All rights reserved.
doi:10.1016/j.snb.2009.11.051

environment have been first time theoretically analyzed by us using Langmuir isotherm kinetic model and Gibbs free energies were calculated for both adsorption–desorption processes. The relative sensitivity of ZnO nanoparticles-based sensor under varying RH values was determined from electrical resistance measurements.

2. Experimental

2.1. Synthesis of ZnO nanoparticles

1 M *X* solution consisting of 0.8 g NaOH and 20 ml C_2H_5OH and 0.084 M *Y* solution consisting of 0.918 g $Zn(CH_3COO)_2$ and 60 ml C_2H_5OH were stirred by magnetic stirring at the 70 °C for 30 min, separately. *Z* solution was prepared stirring *X* and *Y* solution for 30 min in an ice-bath. The precipitation ZnO from solution was carried out by addition of *n*-heptane. The ratio of volume of *n*-heptane to sol was 3:2. After the reaction completed, the resulted white products were centrifugalized and re-dispersed into ethanol. The removal of the ions possibly remaining in the final product from dispersed ZnO was accomplished by repetitive washing of ZnO with ethanol and *n*-heptane.

2.2. Structural characterization of ZnO nanoparticles

The surface morphology and crystal structure of ZnO nanoparticles were investigated using SEM, and XRD (Cu K_α source), respectively. The surface topography and surface roughness of drop-casted ZnO nanoparticles on a glass substrate were examined with a Solver P47H atomic force microscope (NT-MTD) (Moscow, Russia) operating in tapping mode in air at room temperature. Diamond-like carbon (DLC) coated NSG01 DLC silicon cantilevers (from NT-MTD) with a 2 nm tip apex curvature were used at the resonance frequency of 150 kHz. The Nova 914 software package was used to control the SPM system and for the analysis of the AFM images.

2.3. Humidity sensing capabilities of ZnO nanoparticles

QCM technique is a contactless and non-destructive technique for determining the properties of sensing materials, therefore this technique enables testing the sensing capabilities of materials before device design and development stages.

QCM is based on frequency shift of coated quartz crystal with sensing element due to adsorption of humidity atoms on the surface of the sensing material. The mass change (Δm) on surface of the quartz crystal is calculated by using Sauerbrey equation [15] from the frequency change (Δf)

$$\Delta m = -\frac{A\sqrt{\mu\rho}}{2f_0^2}\Delta f \quad (1)$$

where f_0 is the resonant frequency of the fundamental mode of the QCM crystal, A is the area of the gold disk coated onto the crystal, ρ is the density of the crystal, and μ is the shear modulus of quartz.

A time-resolved electrochemical quartz crystal microbalance (EQCM) with the model of CHI400A Series from CH Instruments (Austin, USA) has been used to measure the change in the resonance frequency of quartz crystals between gold electrodes via both serial and USB interface connected to a computer. The QCM works with oscillation frequencies between 7.995 and 7.950 MHz. The density (ρ) of the crystal is 2.684 g/cm^3, and the shear modulus (μ) of quartz is 2.947×10^{11} g/cm s^2. Around oscillation frequency of 7.995 MHz, a net change of 1 Hz corresponds to 1.34 ng of materials adsorbed or desorbed onto the crystal surface of an area of 0.196 cm^2.

In order to monitor humidity sensing properties, ZnO nanoparticles are ultrasonically dispersed in ethanol and solution was applied on the surface of quartz crystal by drop-casting technique. The drop-casted solution was dried using argon gas until ethanol was totally evaporated. The film thickness was measured around 300 nm using both a Dektak profilmeter and AFM cross-section technique. The quartz crystal loaded with ZnO nanoparticles was placed into the Teflon housing and the reference frequency was recorded.

Fig. 1 shows the experimental setup to measure the adsorption (a) and desorption (b) kinetics of drop-casted ZnO nanoparticles under water vapor at the open end of 50 ml water filled volumetric flask using QCM electrodes and a commercial humidity sensor. A T-like pipe was used to divide the humidity equally to measure both signals coming from QCM and RH sensor simultaneously during the adsorption process. Then, the same ZnO nanoparticles covered QCM electrode surface and the commercial RH sensor were exposed to the ambient air (~23 °C and ~ 45% RH) during desorption process. Both the relative humidity and temperature was recorded during measurements to maintain the temperature constant and monitor the varying RH values.

2.4. Relative sensitivity of the ZnO nanoparticle humidity sensor

The ZnO nanoparticle-based sensors were prepared using drop-casting method between thermally evaporated gold electrodes with 30 μm separation and 300 μm channel width on a glass substrate for electrical resistance measurements therefore ZnO nanoparticles bridged the two neighboring gold electrodes. Keithley Sourcemeter was used to measure resistance of the ZnO nanoparticle-based sensor, and the commercial humidity/temperature sensor was used to monitor real-time relative humidity changes during the resistance measurements. The relative sensitivity of ZnO nanoparticle-based sensor was determined by $(R_0 - R)/R_0$, where R_0 is the resistance at ambient air, and R is the resistance at varying relative humidity.

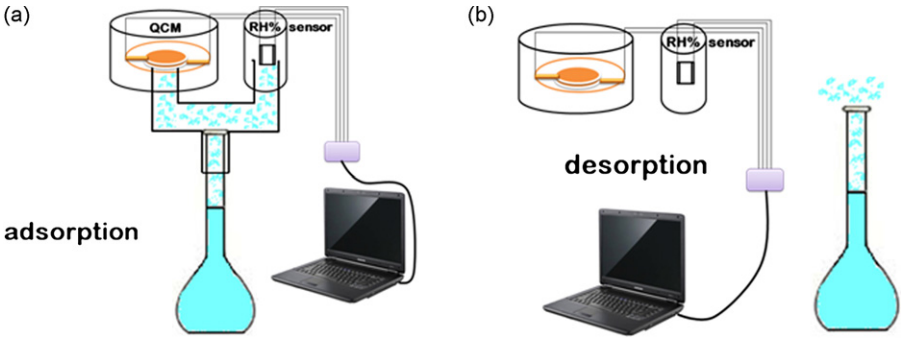

Fig. 1. The experimental setup to measure the adsorption (a) and desorption (b) kinetics of drop-casted ZnO nanoparticles under water vapor at the open end of 50 ml water filled volumetric flask using QCM electrodes and a commercial humidity sensor.

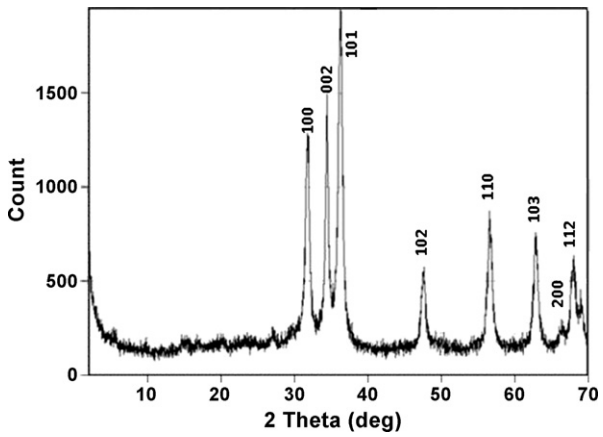

Fig. 2. XRD pattern of the ZnO nanoparticles.

3. Results and discussion

3.1. Structure of ZnO nanoparticles

Fig. 2 shows XRD pattern of synthesized ZnO nanostructures. Diffraction peaks in the XRD pattern are indexed to hexagonal wurtzite structured ZnO (space group $P6_3mc$ (186); $a = b = 0.33$ nm, $c = 0.52$ nm) which agrees well with the JCPDS card (36-1451) and no other diffraction peaks from any kind of side products were observed.

Fig. 3(a–e) shows the optical, AFM and SEM pictures of ZnO nanoparticles at different magnifications. Fig. 3(a) and (b) shows the optical microscopy and AFM images of drop-casted ZnO nanoparticles on the QCM electrodes to give an impression about the morphology and the quality of the drop-casted ZnO layer in large scale, respectively. Fig. 3(c) and (d) shows AFM image and AFM cross-sectional profile of individual ZnO nanoparticles. The SEM images in Fig. 3(e) show the nano-scaled surface properties of the ZnO nanoparticles. The size of the nanoparticles is obtained from both AFM and SEM image analysis. The diameter of the ZnO nanoparticles is measured around 10 ± 3 nm using AFM cross-section techniques over the smallest particles around the edge of ZnO films as shown in Fig. 3(c)–(d). The SEM image given in Fig. 3(e) supports the AFM thickness measurement. The rms surface roughness of the drop-casted ZnO nanoparticles (Fig. 3(b)) from large area (30 μm) was measured around 100 nm by using AFM due to cracks and deep tranches creating porosity on the surface, whereas the rms surface roughness of the ZnO nanoparticles from small regions (less than 500 nm) was obtained around 10 nm. We believe that the large roughness due to cracks on the ZnO film increases the effective area of the ZnO nanoparticles for the adsorption and desorption processes due to possible in and out diffusion of humidity molecules through the cracks.

3.2. QCM results under varying RH

Fig. 4 shows the frequency responses of an empty and loaded QCM with drop-casted ZnO nanoparticles comparing with relative humidity (RH) values of a commercial sensor for 3 humidity adsorption–desorption cycles between 45% and 88% RH. The oscillating resonance frequency of QCM electrodes decreases sharply with increasing RH while there is no change in that of the empty QCM (adsorption process). On the other hand, during the desorption process, the RH is decreased suddenly to the ambient RH value of 45%, as a result, QCM recovers back to its initial resonance frequency value due to desorption of moisture molecules from the drop-casted ZnO nanoparticle surface on the electrodes. The magnitude of change in the oscillating frequency is larger in the first adsorption–desorption cycle compared to the latter repeated cycles due slower desorption rate.

The QCM results show that the ZnO nanoparticles are very sensitive to humidity and give reproducible adsorption and desorption kinetic behavior to humidity changes for short time periods. The ZnO nanoparticles on QCM respond like a commercial RH sensor and can be used for potential humidity sensor application.

3.3. Theoretical analysis of QCM results using modified Langmuir model

Langmuir adsorption isotherm model is frequently used to describe adsorption and desorption kinetics of gas vapor molecules onto organic or inorganic films [16–20]. According to this model, the rate of surface reaction for forming a monolayer on the surface is given by,

$$\frac{d\theta}{dt} = k_a(1-\theta)C - k_d\theta \quad (2)$$

where θ is a unitless quantity, which express the fraction of surface coverage, C is the water vapor concentration (*e.g.*, RH) in the air, k_a and k_d are the rate constants for the adsorption and desorption processes, respectively. In our experiments, the concentration C is proportional to the relative humidity. Hence C is not constant during the adsorption and desorption process but time dependent, $C(t)$. Therefore, solving Langmuir adsorption isotherm equation is not easy analytically. If the time dependent water vapor concentration $C(t)$ is put in place of C, Eq. (2) can be re-written as follows:

$$\frac{d\theta}{dt} = -(k_aC(t) + k_d)\theta + k_aC(t) \quad (3)$$

To solve Eq. (3), QCM result can be used because the frequency shift data measured by QCM is the fractional coverage θ as a function of time during the adsorption and desorption of water vapor molecules on ZnO nanoparticles, while the increase in the frequency shift reflects the molecular mass uptake or loss. Therefore the relationship between the surface adsorption kinetics given by Eq. (2) and frequency shift (Δf) of QCM can be expressed as follows:

$$\frac{d\Delta f}{dt} = -(k_aC(t) + k_d)\Delta f + k_aC(t)\Delta f_{max} \quad (4)$$

Frequency shift (Δf) can be normalized to its maximum value (Δf_{max}) for numerical analysis. The slope and intercept of the least square fitted $d(\Delta f)/dt$ versus Δf line for adsorption–desorption cycles are related to the kinetic constants *i.e.*, slope $= -(k_a \times C(t) + k_d)$ and intercept $= k_a \times C(t)$ to determine adsorption rate k_a and desorption rate k_d as shown in Fig. 5 for the first cycle.

Table 1 shows the fitting parameters ($k_a \times C(t)$ and k_d value) for every cycle determined from the linear fit using Eq. (4) to the experimental data given in Fig. 4. Fig. 6 shows the experimental data and the fit to the Langmuir adsorption and desorption isotherm given in Eq. (3) with the $k_a \times C(t)$ and k_d values obtained from the linear fit for each cycle. As seen from Fig. 6, the fit and the experimental data for Δf versus time are very well-matched.

As seen from Table 1, the product $k_a \times C(t)$ is constant for each cycle. But the vapor concentration $C(t)$ is changing with time due to increase in the relative humidity while keeping the volume constant during the experiment. The pressure does also not change, since the QCM is not sealed to the volumetric flask filled with water. The time dependent change in the vapor concentration of $C(t)$ is the same for each cycle, so that the adsorption rate k_a should be approximately constant. But from the experimental data given in Fig. 6, the maximum frequency change (Δf_{max}) is larger for the first cycle compared to the rest and then it becomes constant. This should be related with the adsorption kinetics of ZnO nanoparticles.

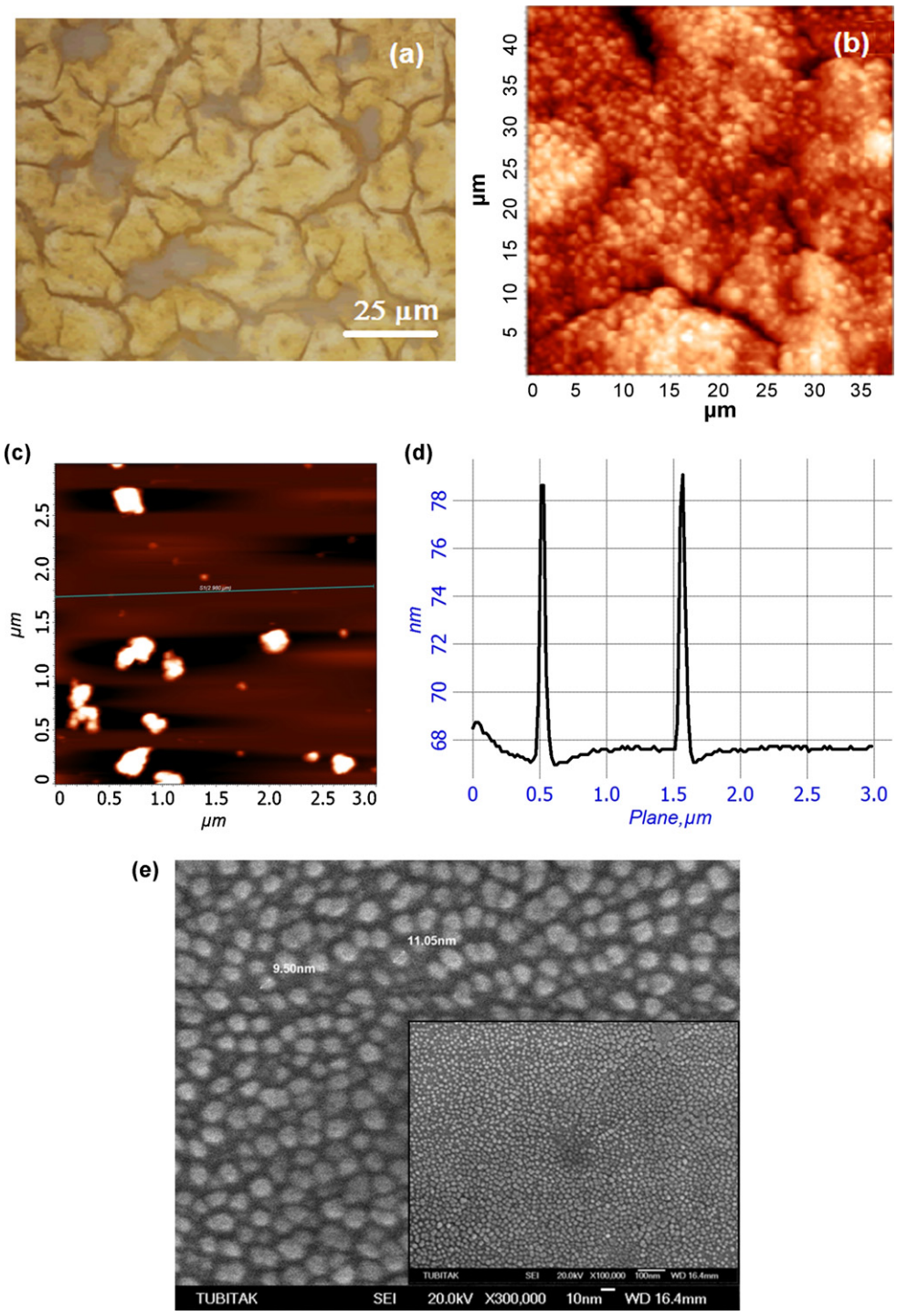

Fig. 3. The ZnO nanoparticles pictures at different magnifications: optical pictures of drop-casted ZnO nanoparticles on the QCM electrodes (a) and AFM image of the surface (b), AFM image and AFM cross-sectional profile of individual ZnO nanoparticles (c) and (d), and SEM images (e).

Table 1
$k_a \times C(t)$ and k_d values determined from the linear fit using Eq. (3) to the experimental data given in Fig. 4 describing adsorption and desorption cycles (with 100 s periods) on the open end of 50 ml water filled volumetric flask.

	1. cycle		2. cycle		3. cycle		Average	
	$k_a\ C(t)\ (s^{-1})$	$k_d\ (s^{-1})$	$k_a\ C(t)\ (s^{-1})$	$k_d\ (s^{-1})$	$k_a\ C(t)\ (s^{-1})$	$k_d\ (s^{-1})$	$k_a\ C(t)\ (s^{-1})$	$k_d\ (s^{-1})$
Adsorption	0.02795	0.00133	0.0139	0.00073	0.0129	0.00036	0.018	0.0008
Desorption	0.0021	0.0394	0.0023	0.0427	0.00136	0.0407	0.0019	0.041

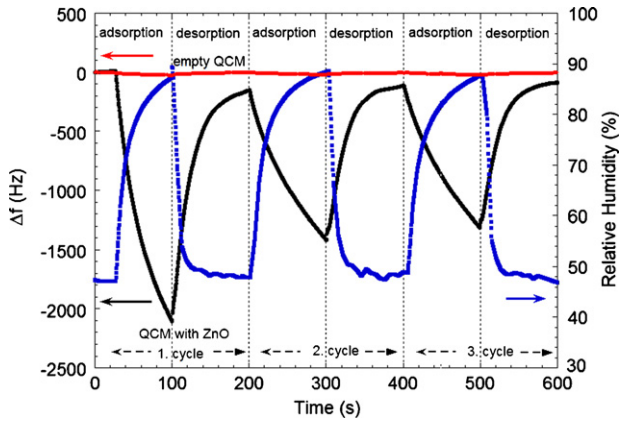

Fig. 4. The frequency relative sensitivities of an empty (red circles) and loaded QCM with drop-casted ZnO nanoparticles (blue squares) comparing with relative humidity values of a commercial sensor (black circles) for 3 humidity adsorption–desorption cycles between 45% and 88% RH. (For interpretation of the references to color in this figure legend, the reader is referred to the web version of the article.)

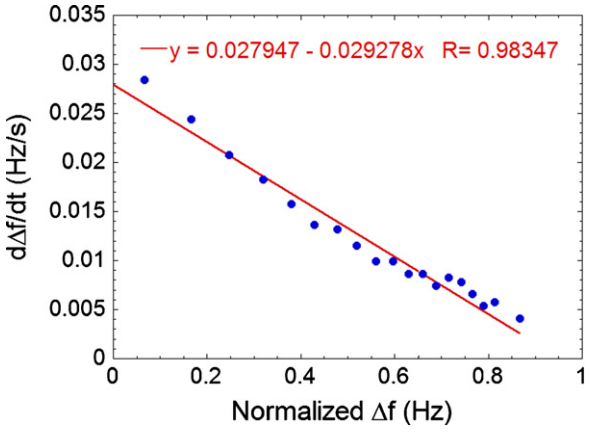

Fig. 5. Plot of d(Δf/dt) versus normalized Δf for adsorption part of first humidity cycle given in Fig. 4.

Fig. 7 shows the experimental data and the fit to the Langmuir adsorption and desorption isotherm given in Eq. (3) with the $k_a \times C(t)$ and k_d values obtained from the linear fit for each cycle. As seen from Fig. 7, the Δf-fit and the experimental data for Δf

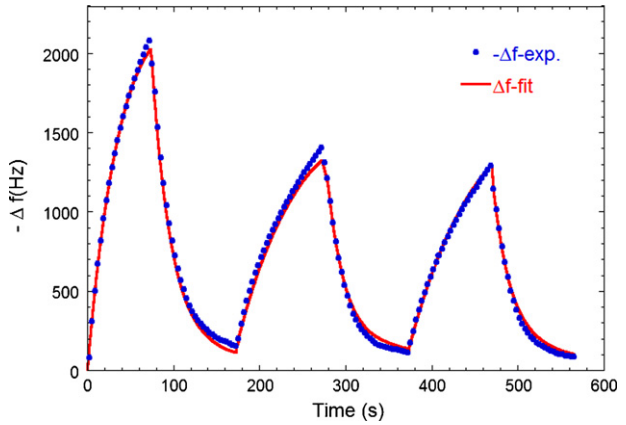

Fig. 6. The experimental data (symbols) and the fit (red solid line) to the Langmuir adsorption and desorption isotherm given in Eq. (3) with the $k_a \times C(t)$ and k_d values obtained from the linear fit for each cycle versus time. (For interpretation of the references to color in this figure legend, the reader is referred to the web version of the article.)

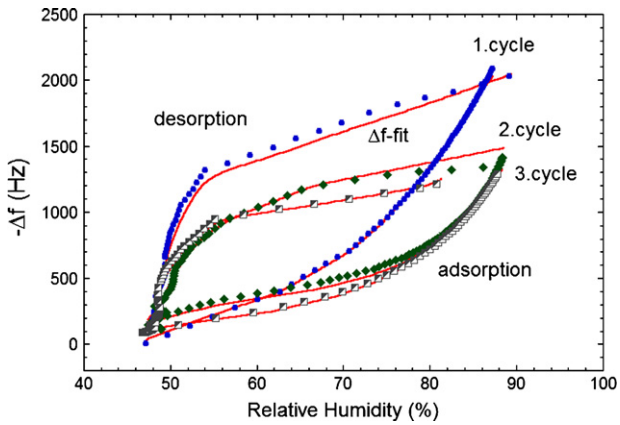

Fig. 7. The experimental data (symbols) and the fit (red solid line) to the Langmuir adsorption and desorption isotherm given in Eq. (3) with the $k_a \times C(t)$ and k_d values obtained from the linear fit for each cycle versus relative humidity. (For interpretation of the references to color in this figure legend, the reader is referred to the web version of the article.)

versus relative humidity are also well-matched. During adsorption process, the QCM frequency shift increases linearly with smaller slope up to a relatively high RH value (75% for cycle 1 and 85% for cycles 2 and 3) compared to initial RH of 45%, and then it increases sharply with increasing slope as a result of mass uptake of QCM plate due to incoming water molecules. During desorption process, the QCM frequency shift decreases linearly with smaller slope up to a relatively small RH value (53% for first cycle and 57% for second and third cycle) compared to initial RH of 45%, and then it decreases abruptly with increasing slope as a result of mass loss of QCM plate due to escaping of water molecules from the surface. The maximum frequency shift for the first cycle is higher than the other cycles again due to initially completely open adsorption sites. However, the maximums of second and third cycles are very close to each other showing equilibrium for the number of adsorption sites.

The maximum values of the adsorption rate $k_a^{\max}$ for each cycle was obtained for the time when the concentration of water vapor reaches its maximum value $C_{\max}(t)$, *e.g.*, at maximum relative humidity around 88%, since the time dependent rising behavior of the RH inside the QCM and on the RH sensor is the same for each cycle with 100 s periods. From the fitting results given in Table 1, the maximum adsorption rate $k_{a1}^{\max} = 0.032\,s^{-1}$ at the maximum RH of 88% is also larger compared to $k_{a2}^{\max} = 0.016\,s^{-1}$, $k_{a3}^{\max} = 0.014\,s^{-1}$, $k_{a4}^{\max} = 0.0148\,s^{-1}$, that of second, third and fourth cycles, respectively as shown in Fig. 8. Hence there is a correlation between the change in the maximum value of frequency shift $\Delta f_{\max}$ and adsorption rates $k_a^{\max}$ for each cycle. At the beginning of the initial adsorption process, all the surface sites are empty and a fraction of the surface will be occupied by water vapor molecules upon the exposure to moisture. This shows that the initial adsorption rate is larger due to number of available adsorption sites on the ZnO nanoparticles.

After number of periodic short desorption cycles, those adsorption sites are no longer active for adsorption process, so that the rate of adsorption is decreased resulting less water vapor mass uptake, *i.e.*, less amplitude of frequency change $\Delta f_{\max}$ of the ZnO nanoparticle loaded QCM plate. But the adsorption rate becomes constant after a certain amount of time needed for thermodynamic equilibrium. On the other hand, the desorption rate k_d during adsorption process is approximately equal, averaging $0.0008\,s^{-1}$ for each cycle, including the first one. This shows that average adsorption rate is around 20 times of average desorption rate during first part of each cycle showing an adsorption dominant process. Nevertheless, aver-

Table 2
Adsorption and desorption parameters for each cycle shown at Fig. 4 and Gibbs free energy values calculated using Eq. (5).

	1. cycle		2. cycle		3. cycle		Average	
	K_{equ}	ΔG (kJ/mol)	K_{equ}	ΔG (kJ/mol)	K_{equ}	ΔG (kJ/mol)	K_{equ}	ΔG (kJ/mol)
Adsorption	24.62	−7.99	21.92	−7.70	40.83	−9.25	29.12	−8.31
Desorption	0.06	+6.99	0.06	+6.97	0.04	+8.16	0.05	+7.37

age desorption rate is around 20 times of average adsorption rate showing desorption dominant process in the second part of each cycle.

The data given in Table 1 and Fig. 8 allow us to determine the equilibrium constant, K_{equ}, for ZnO nanoparticles as follows:

$$K_{equ} = \frac{k_a^{max}}{k_d} \quad (5)$$

The Gibbs free energy ΔG of adsorption–desorption process in terms of K_{equ} at a given temperature is defined as:

$$\Delta G = -RT \ \ln K_{equ} \quad (6)$$

The Gibbs free energy for both adsorption and desorption process is calculated using Eq. (6) for each cycle and results are given in Table 2. The average Gibbs free energies for adsorption and desorption of three cycles is obtained as −8.31 kJ/mol and +7.4 kJ/mol, respectively. Under humidity exposure, water molecules are condensed at the ZnO nanoparticle surface during adsorption process, therefore there is an energy loss for water molecules on ZnO surface. On the other hand, water molecules escaping from the surface of the ZnO gain energy during desorption process.

As seen from Table 2, there is a negligible difference between Gibbs free energies of two processes. It shows that ZnO surface cannot be completely depleted from water molecules during desorption process at room temperature. This explains the small but detectable decrease in the maximum QCM frequency shift for the adsorption part at every sequential cycle as seen in Fig. 4.

3.4. Relative sensitivity of ZnO nanoparticle-based humidity sensor

In Fig. 9, the relative sensitivity of ZnO nanoparticle-based humidity sensor, $(R_0 - R)/R_0$, where R_0 is the resistance of sample @ 52% RH and R is the resistance at varying RH, is shown versus relative humidity cycles in the range of 52–76% RH. As seen from Fig. 9, the relative sensitivity of the sensor is 55% @ 76% RH at room temperature operation. Both QCM and sensitivity measurements confirm that the ZnO nanoparticles-based humidity sensor is very sensitive to the humidity changes even at room temperature.

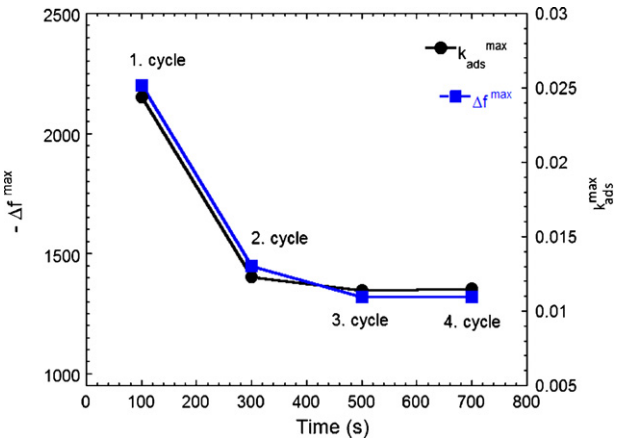

Fig. 8. The maximum values of frequency shift versus adsorption rates k_a^{max} at the maximum RH of 88% for each cycle (4: cycle is not shown in the previous plots).

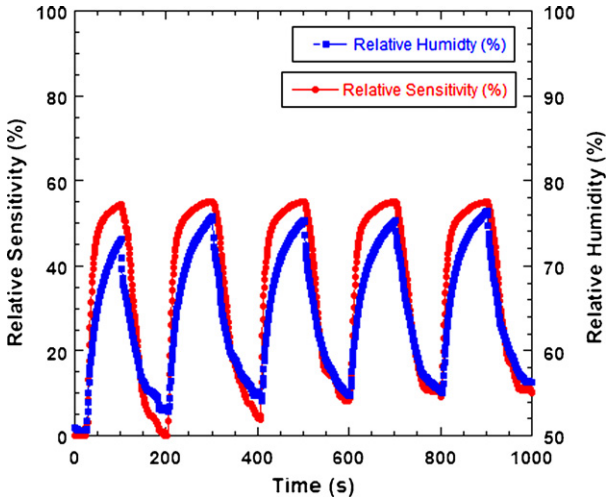

Fig. 9. Relative sensitivity of ZnO nanoparticles-based humidity sensor for the five high-to-low relative humidity cycles.

This kind of behavior of the ZnO nanoparticles-based sensor under varying relative humidity can be explained as follows. It is well-known that ZnO is n-type semiconductor due to localized donor levels in the bandgap caused by oxygen vacancies and interstitial Zn atoms in the lattice. Schaub et al. [21] revealed that the oxygen vacancies are active sites for dissociation of the water molecule using scanning tunneling microscopy experiments and density functional theory calculations. Meyer et al. [22] calculated that the dissociation barrier is very small allowing for an autodissociation of the water molecules even at low temperatures as observed in our experiments carried at room temperature. Oxygen vacancies and surface oxygen ion adsorbed from the air environment on the surface can dissociate water molecule through the transfer of one proton to a nearby oxygen atom, therefore two hydroxyl groups are formed for every oxygen vacancy. The dissociation provides protons as charge carriers of the hopping transport. When the relative humidity increases more, humidity molecules starts to condensate on the surface of the ZnO nanoparticles and both protonic transport and electrolytic conduction contribute to increasing of the sensitivity, *i.e.*, decreasing of the resistance of ZnO nanoparticles-based humidity sensor [13]. The presence of defects, such as steps, more cracked structures increase the surface reactivity drastically. As seen from the optical microscope, AFM and SEM images in Fig. 3, the surface of drop-casted ZnO nanoparticle layer has cracked structure with nano-sized grain morphology therefore more active sites to interact with humidity molecules compared to its bulk counterpart are available in the structure. As a result more adsorbed humidity molecules at the active sites cause decrease at the resistance of the ZnO-based relative humidity sensor.

4. Conclusions

ZnO nanoparticles with about 10 nm diameter were synthesized by sol–gel process. The relative humidity relative sensitivity of ZnO

nanoparticles was investigated by QCM technique. The adsorption and desorption kinetics under varying relative humidity between 45% and 88% were explained using dynamic Langmuir isotherm absorption model. The average Gibbs free energies for adsorption and desorption of three humidity cycles is obtained as −8.31 kJ/mol and +7.4 kJ/mol, respectively. The ZnO nanoparticles-based sensor was fabricated and sensing characteristics to relative humidity were studied. Both QCM and sensitivity results exhibit that the ZnO nanoparticles can be used for fabricating highly sensitive humidity sensors.

Acknowledgement

This work was supported by Research Fund of the Istanbul University. Project number: 2526 and Project number: UDP 3670.

References

[1] D.P. Norton, Y.W. Heo, M.P. Ivill, K. Ip, S.J. Pearton, M.F. Chisholm, T. Steiner, ZnO: growth, doping & processing, Mater. Today 7 (2004) 34–40.
[2] L. Schmidt-Mende, J.L. MacManus-Driscoll, ZnO-nanostructures, defects, and devices, Mater. Today 10 (2008) 40–48.
[3] Z. Fan, J.G. Lu, Nanostructured ZnO: building block for nanoscale devices, Int. J. High Speed Electron. Syst. 16 (2006) 883–896.
[4] H. Ryu, B. Park, S.A. Akbar, W. Lee, K. Hong, Y. Seo, D. Shin, J. Park, G. Choi, ZnO sol–gel derived porous film for CO gas sensing, Sensor. Actuator B 96 (2003) 717–733.
[5] C.S. Rout, S.H. Krishna, S.R.C. Vivekchand, A. Govindaraj, C.N.R. Rao, Hydrogen and ethanol sensor based on ZnO nanorods, nanowires, and nanotubes, Chem. Phys. Let. 418 (2006) 586–590.
[6] C. Xiangfeng, J. Dongli, A.B. Djurisic, Y.H. Leung, Gas-sensing properties of thick film based on ZnO nano-tetrapods, Chem. Phys. Lett. 401 (2005) 426–429.
[7] Y. Lv, L. Guo, H. Xu, X. Chu, Gas sensing properties of well-crystalline ZnO nanodots grown by simple route, Phys. E 36 (2007) 102–105.
[8] J.J. Delaunay, N. Kakoiyama, I. Yamada, Fabrication of three-dimensional network of ZnO tetrapods and its response to ethanol, Mater. Chem. Phys. 104 (2007) 141–145.
[9] Y. Zhang, K. Yu, S. Ouyang, L. Luo, H. Hu, Q. Zhang, Z. Zhu, Detection of humidity based on quartz crystal microbalance coated with ZnO nanostructure films, Phys. B 368 (2005) 94–99.
[10] X. Zhou, J. Zhang, T. Jiang, X. Wang, Z. Zhu, Humidity detection by nanostructured ZnO: a wireless quartz crystal microbalance investigation, Sensor. Actuator A 135 (2007) 209–214.
[11] X. Wang, J. Zhang, Z. Zhu, J. Zhu, Humidity sensing properties of Pd^{2+}-doped ZnO tetrapod, Appl. Surf. Sci. 235 (2007) 3168–3173.
[12] B.C. Yadav, R. Srivastava, C.D. Dwivedi, P. Pramanik, Moisture sensor based on ZnO nanomaterial synthesized through oxalate route, Sensor. Actuator B 131 (2008) 216–222.
[13] Y. Zhang, K. Yu, D. Jiang, Z. Zhu, H. Geng, L. Luo, Zinc oxide nanorod and nanowire for humidity sensor, Appl. Surf. Sci. 242 (2005) 212–217.
[14] J. Xu, Q. Pan, Y. Shun, Z. Tian, Grain size control and gas sensing properties of ZnO gas sensor, Sensor. Actuator B 66 (2000) 277–279.
[15] G. Sauerbrey, Verwendung von Schwingquarzcn zur Wagung d nner Schichten und zur Mikrowagung, Z. Phys. 155 (1959) 206–222.
[16] D.S. Karpovich, G.J. Blanchard, Direct measurement of the adsorption kinetics of alkanethiolate self-assembled monolayers on a microcrystalline gold surface, Langmuir 10 (1994) 3315–3322.
[17] S.J. Gregg, K.S. Sing, Adsorption, Surface Area and Porosity, Academic Press, London, 1967, ISBN 0-12-300956-1.
[18] Y.L. Sun, R.J. Wu, Y.C. Huang, P.G. Su, M. Chavali, Y.Z. Chen, C.C. Lin, In situ prepared polypyrrole for low humidity QCM sensor and related theoretical calculation, Talanta 73 (2007) 857–861.
[19] P.G. Su, Y.P. Chang, Low Humidity sensor based on a quartz-crystal microbalance coated with polyprrole/Ag/TiO_2 nanoparticles composite thin films, Sensor. Actuator B 129 (2008) 915–920.
[20] K. Oura, V.G. Lifshits, A.A. Saranin, A.V. Zotov, M. Katayama, Surface Science: An introduction, Springer, Berlin, 2003.
[21] R. Schaub, P. Thostrup, N. Lopez, E. Laegsgaard, I. Stensgaard, J.K. Norskov, F. Besenbacher, Qxygen vacancies as active sites for water dissociation on rutile TiO_2(1 1 0), Phys. Rev. Lett. 87 (2001), 26104-1–266104-2.
[22] B. Meyer, H. Rabaa, D. Marx, Water adsorption on ZnO (10$\bar{1}$0): from single molecules to partially dissociated monolayers, Phys. Chem. Chem. Phys. 8 (2006) 1513–1520.

Biographies

A. Erol received her Doctor of Philosophy degree in Physics from Istanbul University, Turkey in 2002. Her PhD thesis work focused mainly on electrical and optical characterization of hot electron light emitting devices. During her PhD she also has been at Essex University, UK working on the dilute nitride semiconductors as a visiting fellow. Currently, Ayşe Erol is working at Physics Department of İstanbul University as an Associated Professor. Ayşe Erol's scholarly output includes papers mainly focused on optical and electrical properties of low dimensional III–V group semiconductors, and synthesis of II–VI semiconductor nanostructures as an additional research work, a refereed international conference proceeding, an edited book published by Springer in 2008 and a popular physics book published in 2006.

S. Okurreceived his bachelor's degree in Physics Education from Hacettepe University in Ankara, Turkey in 1989, his master's degree in Physics from Ankara University in Ankara, Turkey in 1992, and master's degree in Physics from Illinois Institute of Technology (IIT) in Chicago, Illinois, USA in 1996, and his PhD in Physics from IIT in 1998. He is currently an Associate Professor in the Department of Physics at Izmir Institute of Technology in Izmir, Turkey. His current research interests include SAM, LB, organic semiconducting thin film interfaces and their application to electronic devices such as organic photovoltaics, OLEDs, OTFTs, nano-dots, nano-wires.

B. Comba received his Bachelor of Science in Physics from Istanbul University, Istanbul, Turkey in 1997. He has been studying on nanostructure synthesizing and investigation of sensor properties of nanostructure as the content of his Master of Science thesis.

Ö. Mermer received his bachelor's degree and his master's degree in Electrical and Electronics Engineering from Ege University (Turkey) in 1998 and 2001, respectively, and his PhD in Physics from Iowa University (USA) in 2006. He is currently Associate Professor in Electrical and Electronics Engineering Department at Ege University (Turkey). His current research interests include magnetic effect in organic semiconductor devices such as OMARs, OLEDs, OTFTs; organic spintronics and sensor applications.

M.Ç. Arıkan received his PhD degree from University of Essex, UK in 1980. His PhD thesis focused on mainly investigation of photoconductive properties of GaAs. Currently Çetin Arıkan is with İstanbul University as a Professor of Solid State Physics, he is actively continuing his research on characterizations and applications of the low dimensional semiconductors. His scholarly output includes papers published in refereed international journals, and refereed international conference proceedings. He is a member of Turkish Physical Society, Institute of Physics UK, and American Physical Society, USA.